Supporting Information

Boosting $BiVO_4$ Photoanode Performance via Organic-Inorganic Cocatalyst Synergy for Efficient Water Splitting

Jiabao Ge[a], Kaige Tian[a], Lingjiang Kong[a], Yu Chen[b] and Junqing Yan*[a]

[a] Key Laboratory of Applied Surface and Colloid Chemistry Ministry of Education.

Shaanxi Engineering Lab for Advanced Energy Technology School of Materials Science and Engineering. Shaanxi Normal University. Xi'an 710119, P. R. China

[b] Institute of High Energy Physics, Chinese Academy of Sciences. 19B Yuquan Road, Shijingshan District, Beijing, China

* Corresponding author. E-mail: junqingyan@snnu.edu.cn

Experimental Procedures

Materials:

All raw materials used in this work were commercially available and required no further purification prior to use. $Bi(NO_3)_3 \cdot 5H_2O$ (98%) was purchased from Alfa Aesar. KI (99.9%), p-benzoquinone (99%), hydrated ruthenium(III) chloride (99%), $FeCl_3 \cdot 6H_2O$ (99%), $VO(acac)_2$ (99%), thiophene-3,4-dicarboxylic acid (99%) and $NiCl_3 \cdot 6H_2O$ (99.99%) were all purchased from Beijing InnoChem Technology Co., Ltd. KOH (90%), Na_2SO_3 (96%), Na_2SO_4 (98%), HNO_3 (69%), DMSO (99.5%), anhydrous ethanol (99.5%) were purchased from Sinopharm Chemical Reagent Co., Ltd. Fluorine-doped tin dioxide (FTO) coated glass (< $15\Omega sq^{-1}$, thickness: 2.2 mm) was obtained from Japan Flat Glass Co., Ltd. All experiments were conducted using deionized water (18.2 MΩ cm).

Synthesis of $BiVO_4$ photoanodes:

In this experiment, the $BiVO_4$ photoanode was prepared by the standard electrodeposition method. First, 3.3200 g of KI, 0.9701 g of $Bi(NO_3)_3 \cdot 5H_2O$ were dissolved in 50 mL of deionized water. Then a certain amount of dilute HNO_3 was added to adjust the pH to 1.7. We use the prepared solution as an A solution. After that, 0.4973 g of p-benzoquinone was weighed and dissolved in 20 mL of absolute ethanol as the B solution. The solutions of A and B were mixed and stirred well to serve as a plating solution. The plating process used a three-electrode system with platinum (Pt) wire as the counter electrode, FTO (F-doped SnO_2) as the functional electrode, and Ag/AgCl as the reference electrode. The working potential was set to -0.1 V vs. Ag/AgCl, and the plating time was controlled to three minutes. Weigh out 0.0300 g of vanadyl acetylacetonate ($VO(acac)_2$) and dissolve it in 2 mL of dimethyl sulfoxide (DMSO) as a C solution. Immediately after, 100 μL of C solution was added drop-wise to each BiOI sample. Then, the sample to which the C solution has been added drop-wise is placed in a tube furnace at 450 °C for two hours at a constant temperature, and the heating rate is set to 2 $°C \cdot min^{-1}$. Finally, to remove the residual V_2O_5 on the surface, we soaked the calcined product in 1 M KOH for one hour. After washing with water and alcohol and drying with N_2, we obtained the target product $BiVO_4$.

Synthesis of $BiVO_4$/TDA photoanodes:

Pre-treat the $BiVO_4$ with 0.01 M dilute nitric acid for 30 seconds to remove surface contaminants and promote hydroxyl group (-OH) growth. Prepare the TDA solution by dissolving 0.05 M TDA in 40 mL of a 1:1 mixture of water and acetonitrile. The acid-treated $BiVO_4$ photoanode is rinsed with deionized water and ethanol to remove residual nitric acid. After drying with N_2, it is immersed in the TDA solution and reacted at room temperature for 12 hours. The sample is then rinsed with deionized water and ethanol, dried with N_2, yielding the $BiVO_4$/TDA photoanode.

Synthesis of $BiVO_4$/TDA/$NiFe_2O_4$ photoanodes:

Dissolve 0.2908 g of $NiCl_2 \cdot 6H_2O$ and 0.808 g of $FeCl_3 \cdot 6H_2O$ in a solution prepared with 3 mL of ammonia water and 37 mL of ethanol. Sonicate to enhance dissolution. The solution was then placed in a PTFE vessel and reacted at 180°C for 12 hours. The reaction product was washed three times with deionized water and ethanol, centrifuged, and vacuum-dried at 60°C for 10 hours to obtain $NiFe_2O_4$. Dissolve $NiFe_2O_4$ in water and sonicate to prepare a 0.5 M suspension. Apply this suspension to a $BiVO_4$/TDA photoanode via spin coating at 3000 rpm for 1 min. After three spin coating cycles, dry the sample at 100°C to obtain the $BiVO_4$/TDA/$NiFe_2O_4$ photoanode. It is worth noting that the loading amount of $NiFe_2O_4$ is approximately 5.9 mg cm^{-2}.

Characterization:

The surface morphology of the detected samples was completed by scanning electron microscopy (SEM, Hitachi-SU8020). Transmission electron microscopy (TEM) was performed on a FEI Tecnai G2F20 electron microscope at an acceleration voltage of 200 kV. To obtain the crystal structures, X-ray diffraction (XRD) spectra were conducted on a Rigaku Smartlab diffractometer with Cu Kα radiation as the X-ray source, and the testing range was 10 - 90° with a scan rate of 0.2°s^{-1}. Raman spectroscopy was carried out using the Renishaw (in Via Reflex) Raman device equipped with a 532 nm laser with a power of 5.0 mW. X-ray photoelectron spectroscopy (XPS) and ultraviolet photoelectron spectroscopy (UPS) were performed on a Thermo Scientific Escalab Xi^+ X-ray photoelectron spectrometer equipped with a monochromated Al Kα X-ray source and operated at 15 kV and 10 mA using C1s at

284.8 eV as the calibration reference. The light absorption abilities and bandgaps of all samples were measured by UV-vis absorption spectra (Hitachi-UH4150) with $BaSO_4$ as the reference. The photoluminescence (PL) spectra were measured by a PICOQUANT-FluoTime300 time-resolved spectrometer with an excitation wavelength of 375 nm. chopper (SR540, Stanford Research Systems, Inc.), and a sample chamber. The sample was sandwiched between two indium tin oxide (ITO) glass electrodes, which were arranged in an atmosphere-controlled container with a quartz window.

Photoelectrochemical Test:

All photoelectrochemical tests in this experiment were performed on a CHI760E-type electrochemical workstation in a typical three-electrode system, with the photoanode as the working electrode, the platinum plate as the counter electrode, and the Ag/AgCl electrode as the reference electrode. A PLS-FX300HU 300 W xenon lamp (with an AM 1.5 G filter) from Beijing Perfectlight Technology Co., Ltd. was used as the simulated solar light source, and a 0.5 M KBi solution (pH = 9.2) was used as the electrolyte. Linear sweep voltammetry (LSV) curves were obtained using linear sweep voltammogram in a voltage window of 0 V ~ 1.23 V vs. RHE with a scan rate of 10 mVs^{-1}. The Mott-Schottky (MS) curve was obtained in the dark with the following parameters: increment 20 mV, frequency 1000 Hz, amplitude 0.005 V vs. Ag/AgCl. Electrochemical impedance spectroscopy (EIS) was collected with an AC voltage amplitude of 5 mV at a DC bias of 1.23 V vs. RHE under AM 1.5 G illumination (frequency range: 0.1 Hz - 100 kHz). The bulk phase charge separation efficiency (η_{bulk}) and surface charge injection efficiency ($\eta_{surface}$) were measured in 0.5 M KBi with the addition of 0.2 M Na_2SO_3. The incident photon to current efficiency (IPCE) of each wavelength was obtained using the illumination from a 300 W Xe lamp. The monochromatic light was produced using a monochromator. The intensity modulated photo-current spectroscopy (IMPS) was tested using an LED source and an Ametek-Modulab XM with a frequency range of 5 KHz to 100 KHz. The superimposition of sinusoidal modulation of ac light was set to ~10% of the dc light. CIMPS were performed in the voltage range of 0.6 V - 1.0 V vs. RHE under 100 mW cm^{-2} LED

illumination. Oxygen evolution was evaluated in an air-tight cell at 1.23 V vs. RHE under AM 1.5 G illumination, and the amounts of gases was measured with a gas chromatograph (Agilent) every 60 min.

All results in this work were presented against the reversible hydrogen electrode (RHE) for ease of comparison with H_2 and O_2 redox levels and other reports that used electrolytes with different pH conditions. The conversion between potentials vs. Ag/AgCl and vs. RHE is performed using the Nernst equation：

$$E_{RHE}=E_{Ag/Cl}+ 0.059\ pH + E^0_{Ag\ /AgCl}$$

E_{RHE} is the potential vs. RHE, $E_{Ag/AgCl}$ is the potential vs. Ag/AgCl, and the value of $E^0_{Ag/AgCl}$ is 0.197 V at 25 ℃.

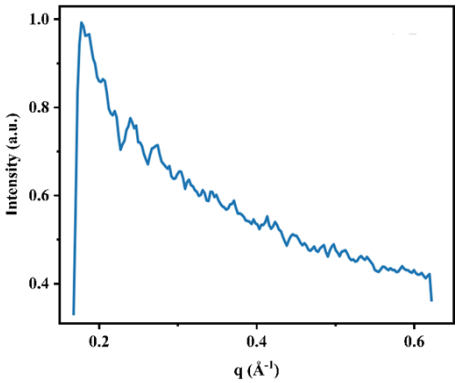

Figure S1. 1D line cuts with q-positions and corresponding d-spacings.

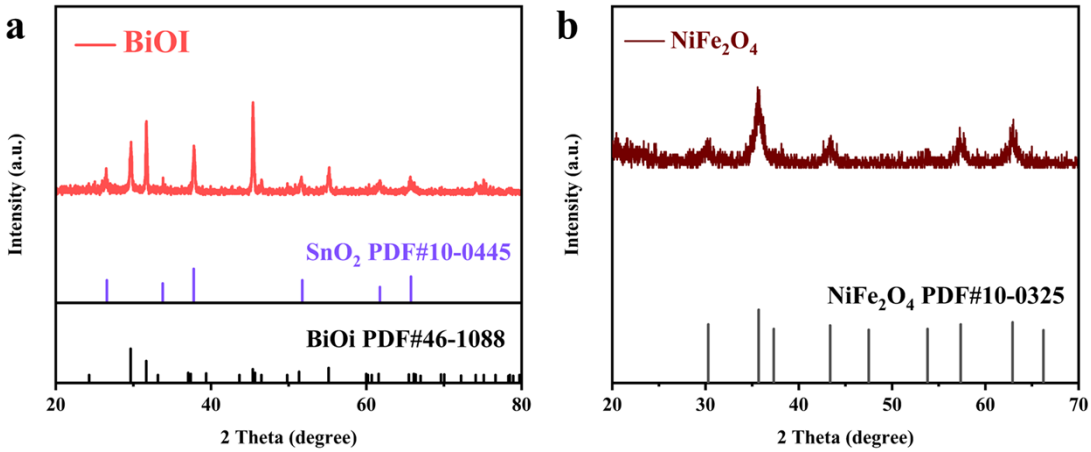

Figure S2. (a) XRD pattern of BiOI. (b) XRD pattern of $NiFe_2O_4$.

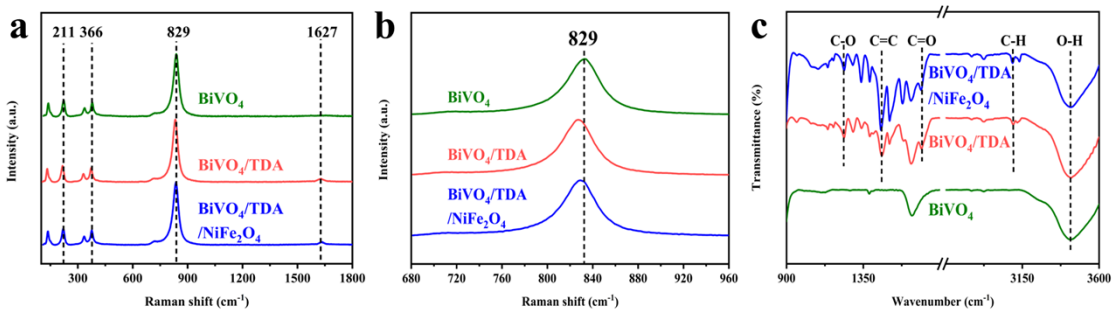

Figure S3. (a) Raman spectrum of all photoanodes. (b) Close-up image of the Raman spectrum of all photoanodes. (c) FTIR spectrum of all photoanodes.

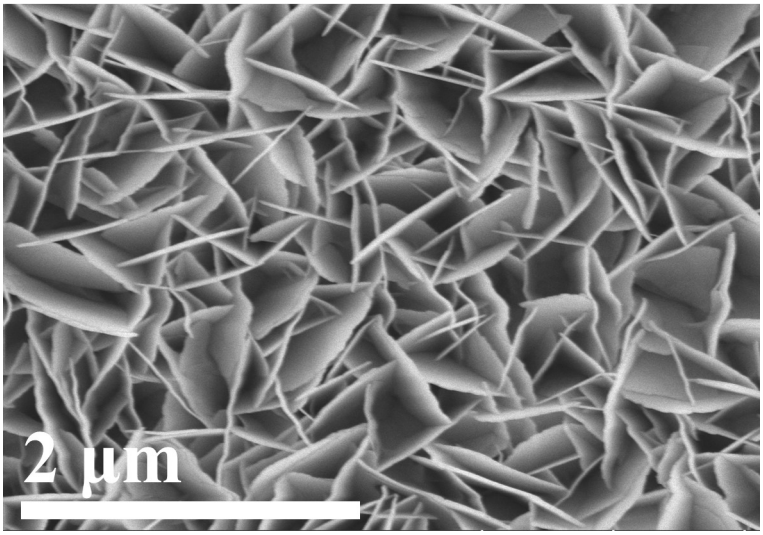

Figure S4. SEM image of BiOI.

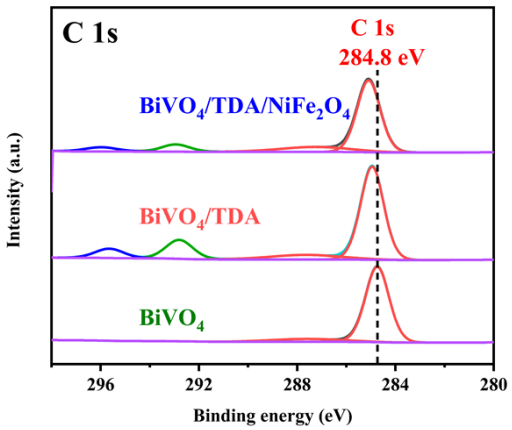

Figure S5. XPS spectrum of the C 1s energy level of all photoanodes.

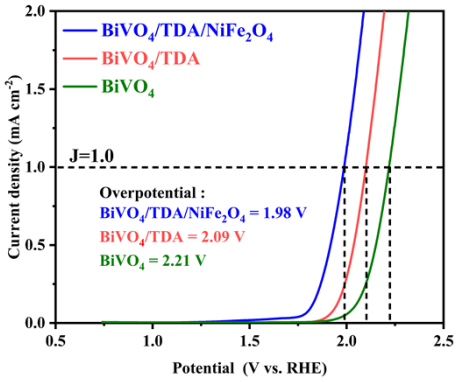

Figure S6. Overpotential of all photoanodes at a current density of 1 mA cm^{-2}.

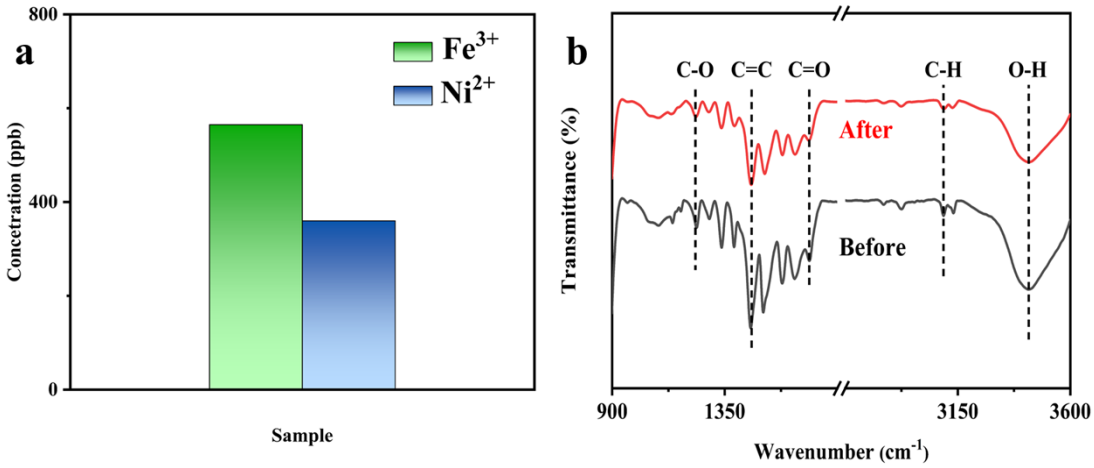

Figure S7. (a) ICP-OES analysis of the electrolyte after a 50 h J-t test. (b) FTIR spectrum of $BiVO_4$/TDA/$NiFe_2O_4$ photoanode before and after 50-hour stability testing.

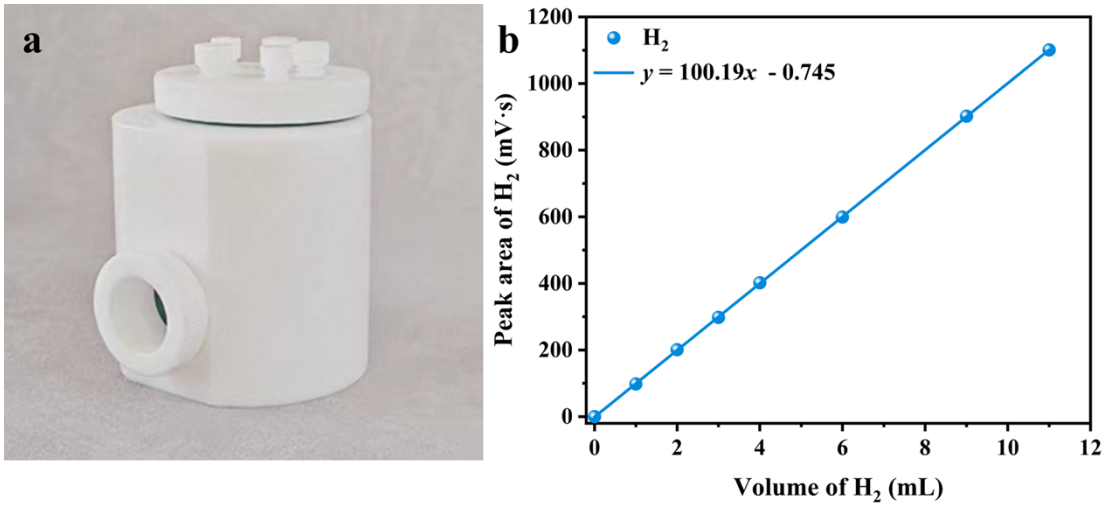

Figure S8. (a) Schematic diagram of the reaction cell. (b) Standard curve for H_2 production by gas chromatography (with argon as carrier gas) equipped with a thermal conductivity detector (TCD).

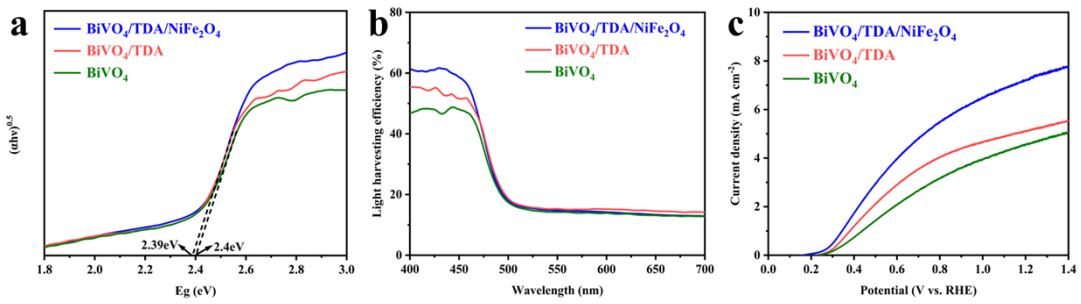

Figure S9. (a) Tauc plots of all photoanodes. (b) Image of LHE values corresponding to different wavelengths of incident light. (c) J_{Na2SO3} of the prepared photoanodes.

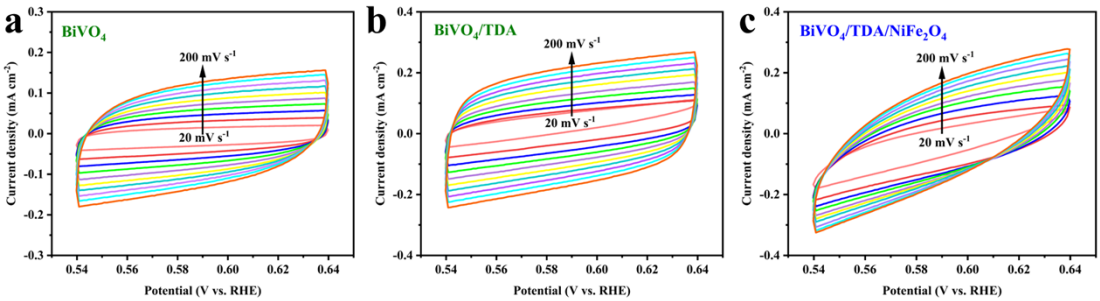

Figure S10. (a) Voltammograms of the $BiVO_4$ photoanode at various scan rates (20 - 200 mV s^{-1}). (b) Voltammograms of the $BiVO_4$/TDA photoanode at various scan rates (20 - 200 mV s^{-1}). (c) Voltammograms of the $BiVO_4$/TDA/$NiFe_2O_4$ photoanode at various scan rates (20 - 200 mV s^{-1}).

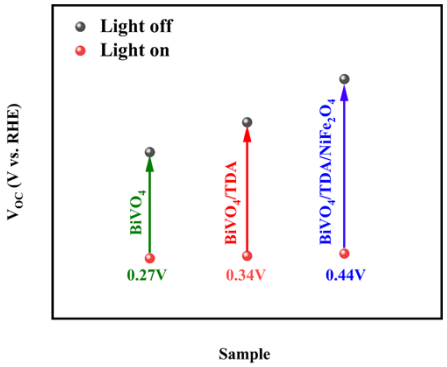

Figure S11. Voltage differences (ΔV_{OC}) based on open-circuit photovoltage tests.

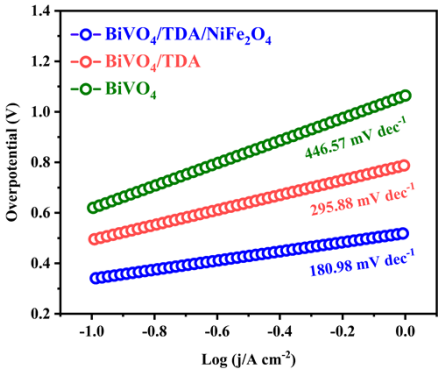

Figure S12. Tafel plots of all photoanodes.

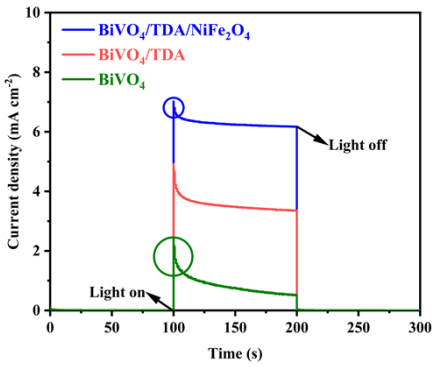

Figure S13. Transient photocurrent curves of all photoanodes.

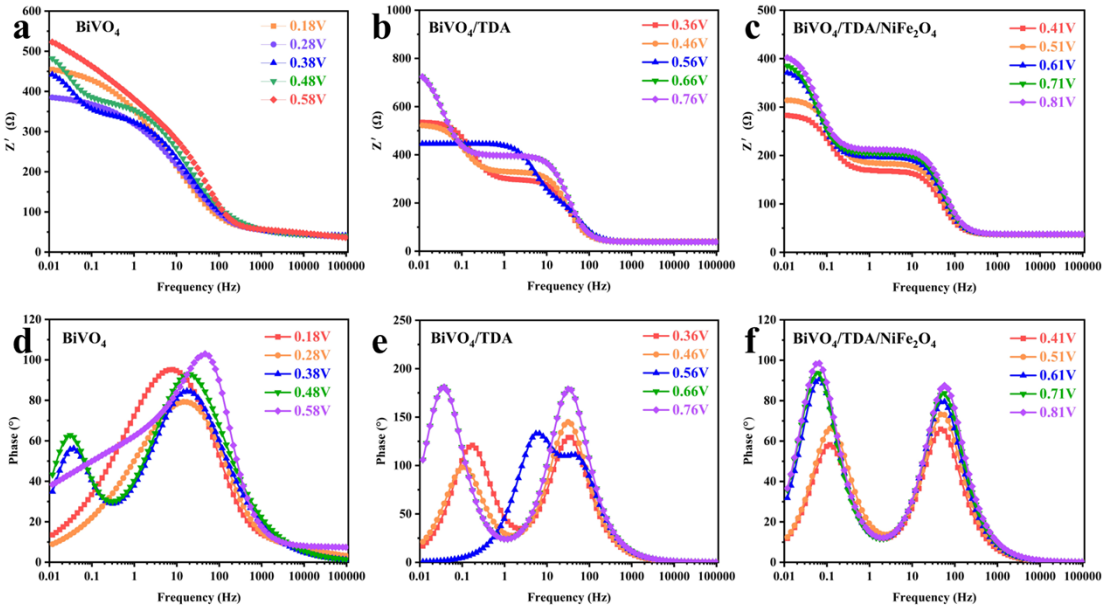

Figure S14. In-situ electrochemical impedance spectroscopy.

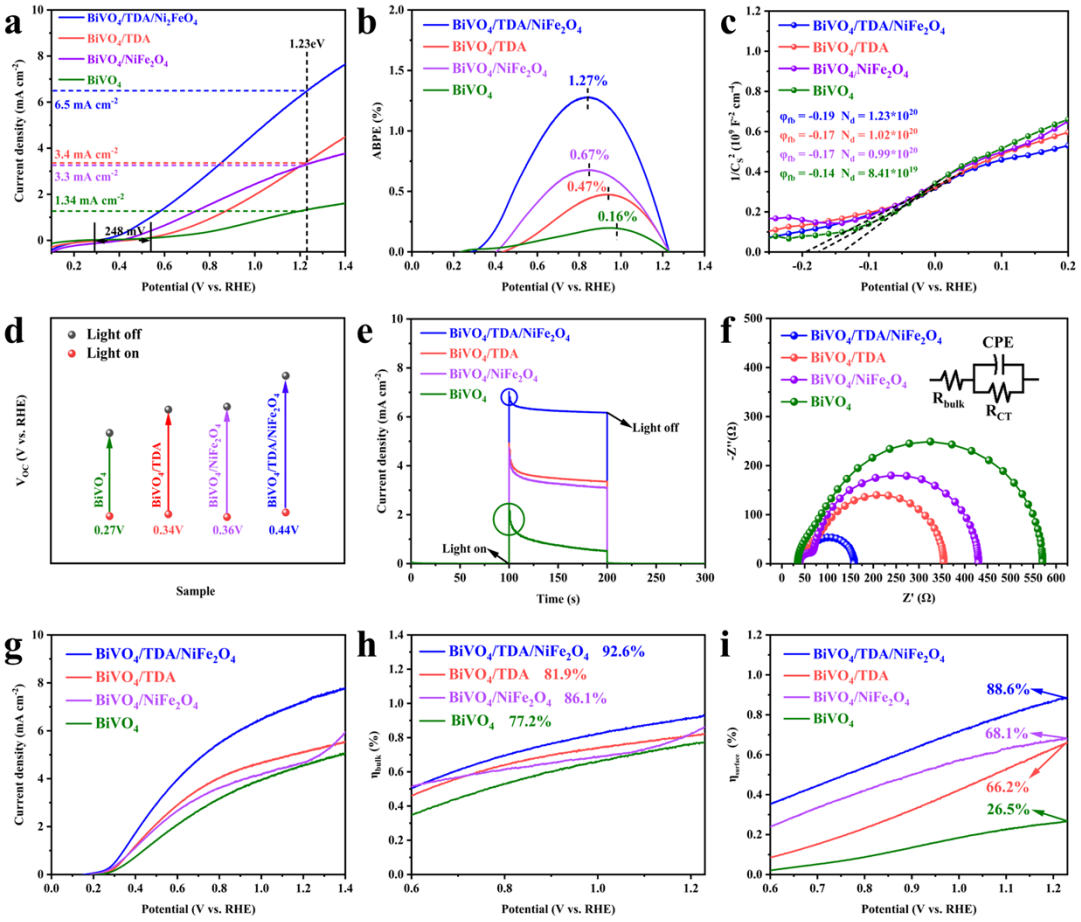

Figure S15. (a) LSV curves. (b) ABPE curves. (c) Mott-Schottky curves of all photoanode. (d) Voltage differences (ΔV_{OC}) based on open-circuit photovoltage tests. (e) Transient photocurrent curves of all photoanodes. (f) Nyquist plots at 1.23 V_{RHE} of all photoanodes. (g) J_{Na2SO3} of the prepared photoanodes. (h) η_{bulk}. (i) $\eta_{surface}$.

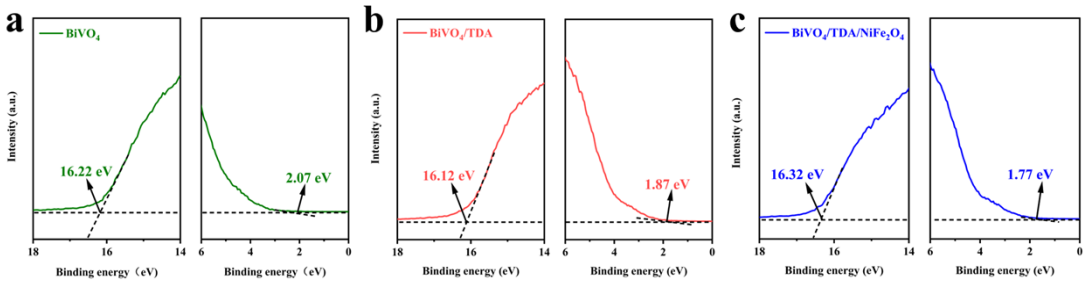

Figure S16. Ultraviolet photoelectron spectroscopy of all photoanodes.

Formula S1:

Applied Bias Photon-to-current Efficiency (ABPE) can be calculated using the following equation:

$$ABPE\ (100\%) = \frac{J \times (1.23 - V_b)}{P_{total}} \times 100\%$$

J refers to the photocurrent density (mA cm^{-2}) obtained from the electrochemical workstation. V_b is the applied bias vs. RHE (V), and P_{total} is the total light intensity of AM 1.5 G (100 mW cm^{-2}).

Formula S2:

The carrier densities are calculated using the following equation:

$$Nd = \frac{2}{e\varepsilon\varepsilon_0} \times \left(\frac{d\left(\frac{1}{C^2}\right)}{dV_S} \right)^{-1}$$

where e is the charge quantity of an electron (1.6×10^{-19} C), vacuum permittivity (ε_0) is 8.86×10^{-12} F m^{-1}, and relative permittivity (ε) is 68 for $BiVO_4$. C (F cm^{-2}) is the space charge capacitance in the semiconductor (obtained from EIS curves), and V_s (V) is the applied potential for M-S curves.

Formula S3:

A gas-tight electrochemical cell coupling with a gas burette was carried out to verify the faradaic yield of all samples (this is the working electrode with the surface area of 1 cm^{-2}). 1.23 V_{RHE} was applied to the electrode, and the volume of the evolved gas was recorded synchronously. Thus, the Faradaic yield was calculated from the ratio of the recorded gas volume to the theoretical gas volume during the charge passed through the electrode:

$$\text{Faradaic yield} = \frac{V_{experimental}}{V_{theoretical}} = \frac{V_{experimental}}{\frac{1}{4} \times \frac{Q}{F} \times V_m}$$

where Q is the charge passed through the electrode, F is Faraday constant (96485 C mol^{-1}), the number 1/4 means 1 mole oxygen per 4 mole electrons, and V_m is the molar volume of gas (24.5 L mol^{-1}, 298 K, 101 KPa).

Formula S4:

The calculation method of bandgap:

$$h\nu = \frac{1240}{\lambda}$$

where λ is the wavelength of the ultraviolet absorption spectrum.

$$y = (\alpha h\nu)^{0.5}$$

Here, y is the bandgap value and α is the absorption intensity in the ultraviolet absorption spectrum.

Formula S5:

The light harvesting efficiencies (LHE, defined as the ratio of absorbed light to the incident sunlight) of each photoanode can be calculated from the UV-vis absorption spectra:

$$LHE = 1\text{-}10^{-A(\lambda)}$$

A(λ) is the absorbance at a specific wavelength.

Formula S6: Theoretical maximum photocurrent density (J_{abs}) is the photocurrent density assuming that all absorbed photons can be converted into current, it is a constant with the AM 1.5 G spectrum and the light harvesting efficiency of the fixed photoelectrode. In the case of J_{abs}, it can be calculated according to the following equation:

$$J_{abs} = \int_{\lambda_1}^{\lambda_2} \frac{\lambda \times LHE(\lambda) \times P(\lambda)}{1240} d(\lambda)$$

where λ and P(λ) are the light wavelength (nm) and the corresponding power density (mW cm^{-2} nm^{-1}) for the standard solar spectrum AM 1.5G (ASTMG-173-03), respectively.

Formula S7:

Bulk charge separation efficiency (η_{sep} or η_{bulk}, the yield of photogenerated holes that have reached the semiconductor/electrolyte interfaces) and surface charge injection efficiency (η_{trans} or $\eta_{surface}$, the yield of holes that are involved in water oxidation reaction after reaching the electrode/electrolyte interfaces) of the as-obtained photoanodes can be calculated using the following equations:

$$\eta_{surface} = \frac{J_{H_2O}}{J_{Na_2so_3}}$$

$$\eta_{bulk} = \frac{J_{Na_2so_3}}{J_{abs}}$$

The theoretical photocurrent density (J_{abs}) is obtained by multiplying the LHE with the AM 1.5 solar spectrum and subsequently integrating it over the appropriate wavelength range on the assumption that the absorbed photon to current efficiency (APCE) is 100%, J_{H2O} and J_{Na2SO3} are the photocurrent densities obtained in 0.5 M KBi electrolyte without and with 0.2 M Na_2SO_3, respectively.

Formula S8:

Then the ECSA was determined by measuring the capacitive current associated with double-layer charging from the scan-rate dependence of CVs. The double-layer capacitance (C_{dl}) was estimated by plotting the $\triangle J = (J_a - J_c)$ at 0.59 V vs. RHE against the scan rate. The linear slope is equivalent to twice of the C_{dl}, which can be used to represent the ECSA.

Formula S9:

Defining the lowest point of the high frequency part of IMPS as f_{IMPS}, the transfer time of photo-generated carriers can be obtained as follows:

$$\tau_{tr} = \frac{1}{2\pi f_{IMPS}}$$

Table S1. Compared the PEC water oxidation performance of $BiVO_4$/TDA/$NiFe_2O_4$ photoanode and other $BiVO_4$-based photoanodes published between 2023 and 2025.

Photoanode	Electrolyte	Current density at 1.23 V_{RHE} (mA cm^{-2})	Ref.
$BiVO_4$/TDA/$NiFe_2O_4$	borate solution	6.5	This work
$NiCoO_x$/Fe-gC_3N_4/$BiVO_4$	phosphate buffer solution	7.4	1
Co_3O_4/CoV-MOF/$BiVO_4$	phosphate buffer solution	6.0	2
NiPt/HfO_2/Ba-$BiVO_4$	phosphate buffer solution	6.5	3
$NiFeO_x$/BVO/$BiVO_4$	phosphate buffer solution	6.4	4
NiOOH/Co_3O_4/$BiVO_4$	borate solution	6.4	5
B:$NiCoO_x$/$BiVO_4$	Formic acid	6.05	6
$BiVO_4$/BPQDs/NiFe-LDHs	phosphate buffer solution	5.28	7
$BiVO_4$/CuS/$NiFeCoO_x$	phosphate buffer solution	6.56	8
$BiVO_4$/VO_x	borate solution	6.29	9

Table S2. The work function (W_F), Fermi level (E_f), valence band maximum (VBM), conduction band minimum (CBM), and bandgap values for the three photoanodes.

Sample	Work function, W_F (eV)	Fermi level, E_f (eV, vs RHE)	VBM (eV, vs RHE)	E_g (eV)	Calculate CBM (eV, vs RHE)
$BiVO_4$	5.0	-5.0	2.63	2.40	0.23
$BiVO_4$/TDA	5.1	-5.1	2.53	2.39	0.14
$BiVO_4$/TDA/$NiFe_2O_4$	4.9	-4.9	2.23	2.39	-0.16

Notes and references

1 Z. Liang, M. Li, K. H. Ye, T. Tang, Z. Lin, Y. Zheng, Y. Huang, H. Ji and S. Zhang, *Carbon Energy*, 2023, **6**. e413.

2 L. Xu, Y. Zhang, B. Liu, K. Wan, X. Wang, T. Wang, L. Wang, S. Wang and W. Huang, *ACS Nano*, 2025, **19**, 15863-15875.

3 M. Arunachalam, K. S. Lee, K. Zhu and S. H. Kang, *Adv. Energy Mater.*, 2024, **14**, 2402607.

4 Z. Xie, D. Chen, J. Zhai, Y. Huang and H. Ji, *Appl. Catal., B Environ. Energy*, 2023, **334**, 122865.

5 Y. Zhang, L. Xu, B. Liu, X. Wang, T. Wang, X. Xiao, S. Wang and W. Huang, *ACS Catal.*, 2023, **13**, 5938-5948.

6 Z. Kang, Y. Zheng, H. Li, Y. Shen, W. Zhang, M. Huang and X. Tao, *Chem. Eng. J.*, 2024, **499**, 156324.

7 Y. Sun, H. Chen, Z. Hou, J. Wang, A. Li and P. F.-X. Corvini, *Chem. Eng. J.*, 2024, **501**, 157662.

8 J. Wang, N. Muhammad, Z. Chuai, W. Xu, X. Tan, Q. Zhou, Y. Yu, J. Guo, T. Li and B. Xu, *Angew. Chem. Int. Ed.*, 2025, **64**, e202507259.

9 B. Liu, X. Wang, Y. Zhang, L. Xu, T. Wang, X. Xiao, S. Wang, L. Wang and W. Huang, *Angew. Chem. Int. Ed.*, 2023, **62**, e202217346.